Light scattering by randomly oriented spheroidal particles

Shoji Asano and Makoto Sato

Light scattering properties of an assembly of randomly oriented, identical spheroidal particles are studied. A computation scheme has been developed to integrate the solution of Asano and Yamamoto for scattering from a homogeneous spheroid over all the particle orientations. The extinction and scattering cross sections, asymmetry factor, and scattering matrix elements are calculated for randomly oriented prolate and oblate spheroids and compared with both calculations for spheres and laboratory measurements. The scattering cross section, single scattering albedo, and asymmetry factor of spheroids tend to be larger than those for spheres of the same volume. The normalized scattering matrix has a symmetrical form with six independent elements. The angular scattering behavior of spheroids is found to be greatly different from that of spheres for side scattering to backscattering directions. In general, prolate and oblate spheroids of the same shape parameter have similar angular scattering patterns. The angular distribution of scattered intensity is characterized by strong forward scattering and weak backscattering. The linear polarization tends to be positive at intermediate scattering angles. The linear polarization and depolarization are discussed in application to scattering in the earth and planetary atmospheres.

I. Introduction

A considerable amount of knowledge of light scattering properties of randomly oriented nonspherical particles has been accumulated from laboratory measurements and field observations on natural atmospheric[1–4] and artificial aerosols,[5–8] ice crystals,[9–11] and hydrosols in seawater.[12,13] On the other hand, theoretical evaluations of the scattering properties have been made only for the special cases of infinitely long circular cylinders,[14] spheroids[15,16] with refractive indices close to 1, and small conducting wires.[17] Several semiempirical[18,19] methods have been proposed to calculate the scattering from randomly oriented, irregular particles. However, the theoretical treatments and the semiempirical methods are still far from reproducing the features in the measurements of the scattering properties of nonspherical particles.

By extending calculations based on the scattering theory developed by Asano and Yamamoto[20] for arbitrarily oriented, homogeneous spheroids, Asano[21] has shown that spheroidal particles provide an excellent opportunity to study the effects of nonspherical particle shapes. Spheroids, formed by rotation of an ellipse about its major (prolate spheroid) or minor (oblate spheroid) axis, can take shapes ranging from needlelike through spherical to platelike.

In this paper we investigate the light scattering properties of an ensemble of randomly oriented, identical spheroidal particles. The extinction and scattering cross sections, asymmetry factors, and elements of the scattering matrix are computed by integrating the solution for a single arbitrarily oriented spheroid over all the orientations in 3-D space. Characteristics of the linear polarization and depolarization will be discussed with relation to applications to scattering in atmospheres. An application to the scattering by freely moving bacterial cells is discussed in a separate paper.[16]

II. Method of Computation

A. Transformation Matrix for the Stokes Parameters

A rigorous solution of electromagnetic wave scattering by homogeneous spheroids is given in Ref. 20. In the theory, the scattered field is expressed in a coordinate system fixed to the spheroid, where the symmetry axis is always in the z axis, and the incident wave vector ${}^{(i)}\mathbf{k}$ lies in the x-z plane with an inclination angle ζ from the z axis. The scattered wave vector ${}^{(s)}\mathbf{k}$ is an arbitrary direction specified by polar angles (θ,ϕ) in the body frame coordinate system. In order to evaluate the scattered field from randomly oriented spheroidal particles, it is convenient to introduce another coordinate system, where ${}^{(i)}\mathbf{k}$ is always coincident with the polar axis or the Z axis. Figure 1 shows the relationship

Both authors were with NASA Goddard Institute for Space Studies, New York, New York 10025, when this work was done; S. Asano is now with Tohoku University, Geophysical Institute, Sendai, 980, Japan.

Received 29 October 1979.
0003-6935/80/080962-13$00.50/0.

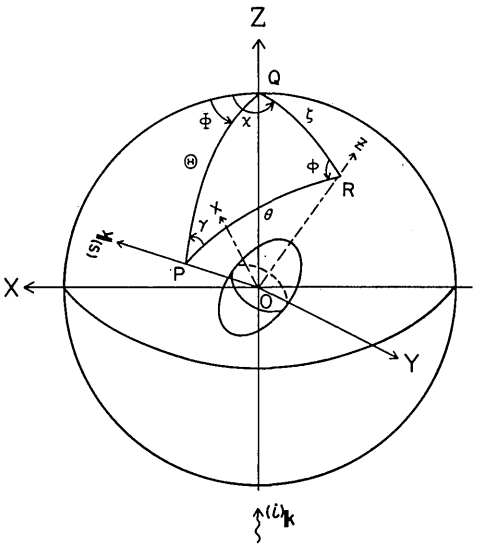

Fig. 1. Geometry of the scattering description for an arbitrarily oriented spheroid in the XYZ coordinate system, where the incident wave vector ${}^{(i)}\mathbf{k}$ is in the polar axis OZ. Orientation of the spheroid is specified by the incidence angle ζ and azimuth angle χ. The direction of scattered wave vector ${}^{(s)}\mathbf{k}$ is defined by the scattering angle Θ and azimuth angle Φ in the XYZ system and by (θ,ϕ) in the body framed system or the xyz coordinate system.

between the two coordinate systems. The orientation of a spheroid or the direction of the symmetry axis of the spheroid is defined by polar angles (ζ,χ) in the XYZ coordinate system.

In the body frame coordinate system, the scattered field at a distance R from the spheroid (in the far field) is related to the incident field by

$$\begin{bmatrix} E_l \\ E_r \end{bmatrix}_{ROP} = \frac{\exp\{i[kR - {}^{(i)}\mathbf{k}\cdot\mathbf{z}]\}}{ikR} \begin{bmatrix} A_2 & A_3 \\ A_4 & A_1 \end{bmatrix} \begin{bmatrix} E_{l0} \\ E_{r0} \end{bmatrix}_{QOR}, \tag{1}$$

where E_l and E_r are the parallel and perpendicular components, respectively, of the scattered field in the scattering plane ROP in the body frame coordinate system, and likewise E_{l0} and E_{r0} are those of the incident field in the incidence plane QOR. The unit vectors $\mathbf{l}$ and $\mathbf{r}$ are, respectively, parallel and perpendicular to a reference plane, and the sense is chosen such that $\mathbf{r}\times\mathbf{l}$ is in the direction of propagation. In Eq. (1), k is the propagation constant in the surrounding medium.

The amplitude functions A_1, A_2, A_3, and A_4 are written, in terms of the amplitude functions in Ref. 20, as

$$\left.\begin{aligned} A_1 &= T_{11}(\theta,\phi) \\ A_2 &= T_{22}(\theta,\phi) \\ A_3 &= -T_{12}(\theta,\phi) \\ A_4 &= T_{21}(\theta,\phi) \end{aligned}\right\}. \tag{2}$$

The scattering process is also described as a linear transformation of the Stokes parameters $[I_0,Q_0,U_0,V_0]$ of the incident light into the Stokes parameters $[I,Q,U,V]$ of the scattered light through the transformation matrix $\mathbf{F}$ by

$$\begin{bmatrix} I \\ Q \\ U \\ V \end{bmatrix}_{ROP} = \frac{1}{k^2R^2}\mathbf{F}(\theta,\phi) \begin{bmatrix} I_0 \\ Q_0 \\ U_0 \\ V_0 \end{bmatrix}_{QOR}, \tag{3}$$

where $\mathbf{F}$ is a matrix of sixteen elements, each of which is a real number and a quadratic expression of the amplitude functions A_1, A_2, A_3, and A_4.[22] We shall define the Stokes parameters, with our choice of time factor $\exp(-i\omega t)$, by

$$\left.\begin{aligned} I &= E_lE_l^* + E_rE_r^* \\ Q &= E_lE_l^* - E_rE_r^* \\ U &= E_lE_r^* + E_rE_l^* \\ V &= i(E_rE_l^* - E_lE_r^*) \end{aligned}\right\}, \tag{4}$$

where an asterisk denotes the conjugate complex values. For this convention of the Stokes parameters, the transformation matrix is written, in the van de Hulst notation,[22] as

$$\mathbf{F} = \begin{bmatrix} \tfrac{1}{2}(M_2+M_3+M_4+M_1) & \tfrac{1}{2}(M_2-M_3+M_4-M_1) & & \\ \tfrac{1}{2}(M_2+M_3-M_4-M_1) & \tfrac{1}{2}(M_2-M_3-M_4+M_1) & & \\ & & S_{23}+S_{41} & D_{23}+D_{41} \\ & & S_{23}-S_{41} & D_{23}-D_{41} \\ S_{24}+S_{31} & S_{24}-S_{31} & S_{21}+S_{34} & D_{21}-D_{34} \\ D_{42}+D_{13} & D_{42}-D_{13} & D_{12}+D_{43} & S_{21}-S_{34} \end{bmatrix}. \tag{5}$$

In the XYZ coordinate system, we shall specify the state of polarization of the incident light in the XZ plane or the $\Phi = 0$ plane. The Stokes parameters of the scattered light in a direction $P(\Theta,\Phi)$ in the scattering QOP plane in this system can be derived through the following linear processes: (a) transformation of the Stokes parameters of the incident light for a rotation of the incidence plane from the XZ plane to the QOR plane; (b) solution of the scattering in the body frame system or Eq. (3); and (c) transformation of the Stokes parameters of the scattered light for a rotation of the scattering plane from the ROP plane to the QOP plane. The above processes are expressed in a mathematical form as

$$\begin{bmatrix} I \\ Q \\ U \\ V \end{bmatrix}_{QOP} = \frac{1}{k^2R^2}\mathbf{Z} \begin{bmatrix} I_0 \\ Q_0 \\ U_0 \\ V_0 \end{bmatrix}_{XZ}, \tag{6}$$

and

$$\mathbf{Z}(\Theta,\Phi;\zeta,\chi) = \mathbf{L}(\pi-\gamma)\cdot\mathbf{F}(\theta,\phi)\cdot\mathbf{L}(-\chi), \tag{7}$$

where $\mathbf{L}(-\alpha)$ is the transformation matrix for a rotation of a reference plane by an angle α in the counterclockwise direction seen against the direction of propagation. For our choice of the Stokes parameters, the rotation matrix is written in the form

$$\mathbf{L}(\pi-\alpha)=\mathbf{L}(-\alpha)=\begin{bmatrix}1 & 0 & 0 & 0\\ 0 & \cos 2\alpha & -\sin 2\alpha & 0\\ 0 & \sin 2\alpha & \cos 2\alpha & 0\\ 0 & 0 & 0 & 1\end{bmatrix}. \quad (8)$$

For a given orientation (ζ,χ) of the spheroid, the angles in Eq. (7) can be explicitly written in Θ, ζ, and $(\chi-\Phi)$ with the help of spherical trigonometry. We find

$$\cos\theta=\cos\Theta\cdot\cos\zeta+\sin\Theta\cdot\sin\zeta\cdot\cos(\chi-\Phi), \quad (9)$$

$$\cos\phi=\frac{\cos\Theta\cdot\sin\zeta-\sin\Theta\cdot\cos\zeta\cdot\cos(\chi-\Phi)}{\pm\sin\theta}, \quad (10)$$

$$\cos\gamma=\frac{\cos\zeta\cdot\sin\Theta-\sin\zeta\cdot\cos\Theta\cdot\cos(\chi-\Phi)}{\pm\sin\theta}, \quad (11)$$

where in the last two equations the plus sign should be taken when $0<(\chi-\Phi)<\pi$, and the minus sign should be taken when $\pi<(\chi-\Phi)<2\pi$.

Our goal is to obtain the transformation matrix of the Stokes parameters for the scattering by an ensemble of identical spheroids oriented randomly in a 3-D space. In that case, the scattered field is independent of the azimuth angle Φ. Hence we shall choose the XZ plane as the scattering plane or the reference plane for the Stokes parameters of the incident and scattered light. The Stokes parameters for the total scattered fields due to all the particle orientations are the sum of the stokes parameters for the individual orientations. Then the averaged transformation matrix $\overline{\mathbf{F}(\Theta)}$ for a sample of randomly oriented spheroids can be obtained by integrating the transformation matrix for a particular orientation over all the orientations; thus,

$$\overline{\mathbf{F}(\Theta)}=\frac{1}{4\pi}\int_0^{2\pi}\int_0^{\pi}\mathbf{Z}(\Theta,0;\zeta,\chi)\sin\zeta d\zeta d\chi. \quad (12)$$

The transformation matrix $\overline{\mathbf{F}(\Theta)}$ for randomly oriented spheroidal particles that have a plane of symmetry is a function only of the scattering angle Θ and has the form, with six independent parameters,[22]

$$\bar{\mathbf{F}}=\begin{bmatrix}\bar{f}_{11} & \bar{f}_{12} & 0 & 0\\ \bar{f}_{12} & \bar{f}_{22} & 0 & 0\\ 0 & 0 & \bar{f}_{33} & \bar{f}_{43}\\ 0 & 0 & \bar{f}_{43} & \bar{f}_{44}\end{bmatrix}. \quad (13)$$

This characteristic form of the matrix could be used as an accuracy check of the integration in Eq. (12). In practice, because of the symmetry relationships for an interchange of Φ and χ in Eqs. (9)–(11) and for the amplitude functions $T_{ij}(\pi-\zeta;\pi-\theta,2\pi-\phi)=T_{ij}(\zeta;\theta,\phi)$, the integration in Eq. (12) can be taken only over ζ from 0 to $\pi/2$ and over Φ, instead of χ but setting $\chi=0$, from 0 to π. Assuming a uniform distribution of particle orientations, we evaluated the integral by making the scattering calculation for an increasing number of equally probable orientations until the result coverges.

B. Scattering Cross Section and Asymmetry Factor

The scattering cross section for an assembly of randomly oriented, identical spheroids is defined by

$$\overline{C_{\text{sca}}}=\int_{4\pi} I/I_0R^2d\Omega, \quad (14)$$

where $d\Omega$ is an element of solid angle. From Eqs. (6)–(8), (12), and (13), we have

$$I/I_0=\frac{1}{k^2R^2}\left[\bar{f}_{11}+\bar{f}_{12}\frac{Q_0}{I_0}\right]=\frac{1}{4\pi k^2R^2}\left[\iint f_{11}\sin\zeta d\zeta d\chi+\frac{Q_0}{I_0}\iint(\cos 2\chi\cdot f_{12}+\sin 2\chi\cdot f_{13})\sin\zeta d\zeta d\chi\right], \quad (15)$$

where f_{ij} is the element of the transformation matrix, Eq. (5), in the ith row and jth column. By inserting Eq. (15) into Eq. (14) and exchanging the order of integration, the contribution of the second term of Eq. (15) vanishes, and we have

$$\overline{C_{\text{sca}}}=\tfrac{1}{2}\int_0^{\pi/2}[C_{1,\text{sca}}(\zeta)+C_{2,\text{sca}}(\zeta)]\sin\zeta d\zeta. \quad (16)$$

Here $C_{1,\text{sca}}(\zeta)$ and $C_{2,\text{sca}}(\zeta)$ are the scattering cross sections for the TE and TM mode incidence waves, respectively, at the incidence angle ζ, and their explicit expression is given by Eqs. (116) and (118) in Ref. 20, respectively.

For the averaged extinction cross section $\overline{C_{\text{ext}}}$, we can obtain a similar expression:

$$\overline{C_{\text{ext}}}=\tfrac{1}{2}\int_0^{\pi/2}[C_{1,\text{ext}}(\zeta)+C_{2,\text{ext}}(\zeta)]\sin\zeta d\zeta. \quad (17)$$

The explicit forms of $C_{1,\text{ext}}(\zeta)$ and $C_{2,\text{ext}}(\zeta)$ are given by Eqs. (110) and (111) in Ref. 20. We define the asymmetry factor $\langle\cos\Theta\rangle$ averaged over all the orientations by

$$\overline{\langle\cos\Theta\rangle}\cdot\overline{C_{\text{sca}}}=\int_{4\pi} I/I_0\cos\Theta\cdot R^2d\Omega, \quad (18)$$

where the cosine of the scattering angle Θ is written, from the spherical geometry shown in Fig. 1, in the form

$$\cos\Theta=\cos\zeta\cos\theta+\sin\zeta\sin\theta\cos\phi. \quad (19)$$

Equation (18) can be integrated analytically in the same way as in the case of C_{sca}, and we finally obtain

$$\overline{\langle\cos\Theta\rangle}=\frac{1}{2\overline{C_{\text{sca}}}}\int_0^{\pi/2}\Big\{\cos\zeta[(\langle\cos\Theta\rangle_1C_{1,\text{sca}})_A+(\langle\cos\Theta\rangle_2C_{2,\text{sca}})_A]+\sin\zeta[(\langle\cos\Theta\rangle_1C_{1,\text{sca}})_B+(\langle\cos\Theta\rangle_2C_{2,\text{sca}})_B]\Big\}\sin\zeta d\zeta, \quad (20)$$

where

$$\langle(\cos\Theta)C_{\mathrm{sca}}\rangle_A = \frac{\pi}{k^2}\sum_{m=0}(1+\delta_{0m})\Bigg(\sum_{n=m}\sum_{n'=m}(\alpha_{mn}\alpha^*_{mn'}+\beta_{mn}\beta^*_{mn'})$$
$$\times\Bigg\{\sum_{r=0,1}{}'\frac{2(2m+r)!}{(2m+2r+1)r!}d_r^{mn}\left[\frac{(m+r)(m+r+2)(2m+r+1)}{(2m+2r+3)}d_{r+1}^{mn'}+\frac{r(m+r+1)(m+r-1)}{(2m+2r-1)}d_{r-1}^{mn'}\right]\Bigg\}\Bigg)$$
$$+\frac{\pi}{k^2}\sum_{m=1}\sum_{n=m}m(\alpha_{mn}\beta^*_{mn}+\alpha^*_{mn}\beta_{mn})\left[\sum_{r=0,1}{}'\frac{2(2m+r)!}{(2m+2r+1)r!}(d_r^{mn})^2\right], \tag{21}$$

$$\langle(\cos\Theta)C_{\mathrm{sca}}\rangle_B = \frac{\pi}{2k^2}\sum_{m=0}(1+\delta_{0m})\sum_{n=m}\sum_{n'=m+1}\Bigg\{\Big(\alpha_{mn}\alpha^*_{m+1,n'}+\beta_{mn}\beta^*_{m+1,n'}\Big)$$
$$\times\Bigg\{\sum_{r=0,1}{}'\frac{2(2m+r)!}{(2m+2r+1)r!}d_r^{mn}\left[\frac{(m+r)(m+r+2)(2m+r+1)(2m+r+2)}{(2m+2r+3)}\right.$$
$$\left.\times d_r^{m+1,n'}-\frac{r(r-1)(m+r-1)(m+r+1)}{(2m+2r-1)}d_{r-2}^{m+1,n'}\right]\Bigg\}$$
$$-(\alpha_{mn}\beta^*_{m+1,n'}+\alpha^*_{m+1,n'}\beta_{mn})\left[\sum_{r=0,1}{}'\frac{2r(2m+r+1)(2m+r)!}{(2m+2r+1)r!}d_r^{mn}d_{r-1}^{m+1,n'}\right]\Bigg\}$$
$$+\frac{\pi}{2k^2}\sum_{m=1}(1+\delta_{1m})\sum_{n=m}\sum_{n'=m-1}\Bigg\{(\alpha_{mn}\alpha^*_{m-1,n'}+\beta_{mn}\beta^*_{m-1,n'})$$
$$\times\Bigg\{\sum_{r=0,1}{}'\frac{2(2m+r)!}{(2m+2r+1)r!}d_r^{mn}\cdot\left[\frac{(m+r-1)(m+r+1)}{(2m+2r-1)}d_r^{m-1,n'}-\frac{(m+r)(m+r+2)}{(2m+2r+3)}d_{r+2}^{m-1,n'}\right]\Bigg\}$$
$$-(\alpha_{mn}\beta^*_{m-1,n'}+\alpha^*_{m-1,n'}\beta_{mn})\left[\sum_{r=0,1}{}'\frac{2(2m+r)!}{(2m+2r+1)r!}d_r^{mn}d_{r+1}^{m-1,n'}\right]\Bigg\}. \tag{22}$$

Subscripts 1 and 2 in Eq. (20) again represent the polarization modes of the incident wave. The notation in Eqs. (21) and (22) is the same as that used in Ref. 20.

Since the scattering and extinction cross sections and the asymmetry factor vary relatively slowly with the incidence angle ζ, Eqs. (16), (17), and (20) can be numerically integrated with a coarser resolution in ζ than can be done in the case of Eq. (12). We evaluated the integrals by means of the Gauss quadrature with 10–15 division points, depending on the size and shape of the spheroids, in the interval $0 \le \zeta \le \pi/2$.

C. Normalized Scattering Matrix

We introduce the normalized scattering matrix $\mathbf{P}(\cos\Theta)$, of which the element in the first row and first column, P_{11}, is the so-called phase function and satisfies the normalization condition:

$$\int_{4\pi}P_{11}(\cos\Theta)d\Omega/4\pi = 1. \tag{23}$$

The normalized scattering matrix $\mathbf{P}$ is proportional to the averaged transformation matrix $\bar{\mathbf{F}}$, and the proportionality constant is found, with the aid of Eqs. (14) and (23), to be $k^2\overline{C_{\mathrm{sca}}}/4\pi$, that is,

$$\frac{k^2\overline{C_{\mathrm{sca}}}}{4\pi}P_{ij} = \bar{f}_{ij} \quad (i,j = 1,\ldots 4). \tag{24}$$

Finally, the scattering from an ensemble of randomly oriented, identical spheroids can be written, in terms of the normalized scattering matrix, as

$$\begin{bmatrix}I\\Q\\U\\V\end{bmatrix} = \frac{\overline{C_{\mathrm{sca}}}}{4\pi R^2}\begin{bmatrix}P_{11} & P_{12} & 0 & 0\\ P_{12} & P_{22} & 0 & 0\\ 0 & 0 & P_{33} & -P_{43}\\ 0 & 0 & P_{43} & P_{44}\end{bmatrix}\begin{bmatrix}I_0\\Q_0\\U_0\\V_0\end{bmatrix}. \tag{25}$$

If we adopt another set of Stokes parameters (I_l,I_r,U,V) instead of (I,Q,U,V) in order to specify the state of polarization of light, the scattering from ransomly oriented spheroids will be described by the normalized transformation matrix $\mathbf{Q}$ in the form

$$\begin{bmatrix}I_l\\I_r\\U\\V\end{bmatrix} = \frac{\overline{C_{\mathrm{sca}}}}{4\pi R^2}\begin{bmatrix}Q_{11} & Q_{12} & 0 & 0\\ Q_{12} & Q_{22} & 0 & 0\\ 0 & 0 & Q_{33} & -Q_{43}\\ 0 & 0 & Q_{43} & Q_{44}\end{bmatrix}\begin{bmatrix}I_{l0}\\I_{r0}\\U_0\\V_0\end{bmatrix}. \tag{26}$$

Note that Q_{12} represents the cross-polarized components for the incidence of light polarized linearly, either parallel or perpendicular to the scattering plane. The elements of the scattering matrix $\mathbf{P}$ are related to the elements of the transformation matrix $\mathbf{Q}$ through the relations

$$\left.\begin{aligned}&P_{11} = \tfrac{1}{2}(Q_{11}+2Q_{12}+Q_{22})\\ &P_{22} = \tfrac{1}{2}(Q_{11}-2Q_{12}+Q_{22})\\ &P_{12} = \tfrac{1}{2}(Q_{11}-Q_{22}),\ P_{33} = Q_{33}\\ &P_{43} = Q_{43},\ P_{44} = Q_{44}\end{aligned}\right\}. \tag{27}$$

III. Computed Results

In this paper we specify the size and shape of prolate and oblate spheroids by the size parameter $\alpha = 2\pi a/\lambda$ and the shape parameter a/b, respectively, where a and b are the semimajor and semiminor axes of the ellipse, and λ is the wavelength of the incident light. In order to compare the scattering from randomly oriented spheroids with that from spheres, we introduce two types of equivalent spheres: one is the sphere of the same volume, and the other is the sphere of the same surface area, or equivalently, of the cross-sectional area equal to the averaged projected area[22,23] of randomly oriented spheroids. Writing r_V and r_G for the radii of the volume and area equivalent spheres, respectively,

Table I. Ratios of the Radii r_V and r_G of the Volume and Area Equivalent Spheres, Respectively, to the Semimajor Axis a of Spheroids

	Prolate		Oblate	
a/b	r_V/a	r_G/a	r_V/a	r_G/a
2	0.62996	0.65368	0.79370	0.83071
3	0.48075	0.52265	0.69336	0.77709
5	0.34200	0.39971	0.58480	0.73946

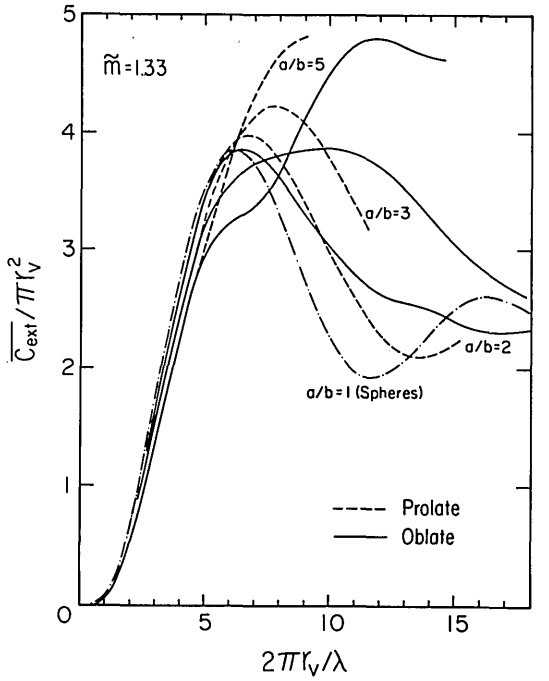

Fig. 2. Averaged extinction cross sections normalized by the cross-sectional area πr_V^2 of the volume equivalent spheres as a function of the equivalent size parameter $2\pi r_V/\lambda$ for randomly oriented prolate and oblate spheroids with the refractive index $\tilde{m} = 1.33$ and the shape parameter $a/b = 2$, 3, and 5. The extinction cross sections for spheres are also shown. For spheres, the size distribution Eq. (28) is used with $r_{eq} = r_V$ and $v_{eff} = 0.01$.

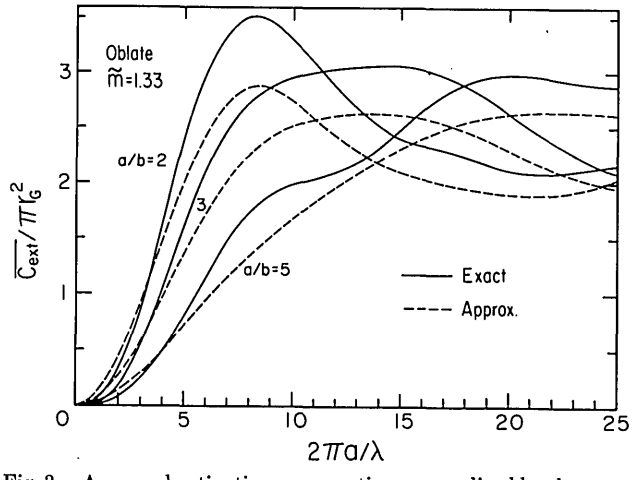

Fig. 3. Averaged extinction cross sections normalized by the cross-sectional area πr_G^2 of the area equivalent spheres or the extinction efficiency factors of randomly oriented oblate spheroids with $\tilde{m} = 1.33$ and $a/b = 2$, 3, and 5 as a function of the size parameter $2\pi a/\lambda$. Values calculated with the anomalous diffraction approximation are compared.

numerical values of the ratios r_V/a and r_G/a are given in Table I for prolate and oblate spheroids of $a/b = 2$, 3, and 5.

Scattering from the equivalent spheres was calculated from the Mie theory. Integration over a narrow size distribution was performed in order to smooth out the oscillations that occur for a single size. The standard size distribution of Hansen and Travis[24] was used in the form

$$n(r) = \text{const} \cdot r^{1-3v_{eff}/v_{eff}} \cdot \exp\left(-\frac{r}{r_{eq}v_{eff}}\right), \tag{28}$$

where $n(r)dr$ is the number of spheres with radius between r and $r + dr$, and r_{eq} is the radius of the equivalent spheres. The effective variance v_{eff} was set to 0.01 or 0.05. For spheroids, integration over size was not necessary since integration over random orientation served the same function. The light scattering properties of spherical particles are extensively reviewed in Ref. 24.

A. Extinction Cross Sections and Asymmetry Factors

Figure 2 shows the averaged extinction cross sections normalized by the cross-sectional area πr_V^2 of the volume equivalent spheres as a function of size parameter $2\pi r_v/\lambda$ for the spheres for randomly oriented prolate and oblate spheroids with refractive index $\tilde{m} = 1.33$. It should be noted that, at large particle sizes, the curves will oscillate about the asymptotic value of $2 \cdot (r_G/r_V)^2$ not 2. For small spheroids, $2\pi r_V/\lambda \lesssim 5$, the extinction cross sections are primarily dependent on volume and weakly dependent on shape. For larger spheroids of sizes larger than that of the first maximum in the extinction cross-section curve for spheres, i.e., $2\pi r_V/\lambda \gtrsim 6$, positions of maxima and minima in the extinction curves shift to larger sizes for larger a/b. The bumps near $2\pi r_V/\lambda \approx 5$ and 12 in the curve for oblate spheroids of $a/b = 5$ are due to an oscillation superimposed on the main oscillation caused from interference effects of light diffracted and transmitted by the spheroids. The superimposed oscillation is more clearly seen in Fig. 3.

In Fig. 3 exact efficiency factors defined by the ratio of the extinction cross section to the averaged projected area are compared to approximate values. The latter were obtained by integrating the expression by Greenberg and Meltzer[25] for the scalar wave scattering cross section of arbitrarily oriented spheroids. This scalar wave treatment is equivalent to the anomalous diffraction approximation of van de Hulst.[22] The figure is for oblate spheroids with $\tilde{m} = 1.33$ and $a/b = 2$, 3, and 5. This kind of comparison is useful not only in estimating errors involved in the approximation but also provides insight regarding the physical mechanism involved in the exact solution. Although the anomalous diffraction approximation has been introduced for spheres in the limiting case of $|\tilde{m} - 1| \ll 1$ and $2\pi r/\lambda \gg 1$,[22] this approximation provides fairly good prediction of the efficiency factors for spheroids in particular orientations, even with $\tilde{m} = 1.33$, e.g., the incidence angle $\zeta \to 90°$ for prolate spheroids and $\zeta \to 0°$ for oblate spheroids, respectively. For other orientations, such as $\zeta \to 0°$ for prolate spheroids and $\zeta \to 90°$

for oblate spheroids, however, the approximation breaks down. This may be attributed to neglect of effects of edge phenomena or grazing reflection.[21,26]

This figure shows that, although the anomalous diffraction approximation overestimates the extinction efficiency factor for small sizes and underestimates it in varying degrees for large sizes, the approximation provides the efficiency curves nicely in phase with those for the exact calculation for randomly oriented spheroids. This fit in phase is because the effect of grazing reflection is diminished by averaging over all the orientations. Because of the factor $\sin\zeta$ in the integral, Eq. (17), particles in orientations with the incidence angle closer to 90° make larger contributions to the average. The effect of grazing reflection is smaller for randomly oriented prolate spheroids than it is for oblate spheroids. Thus the effect of grazing reflection remains evident for thin oblate spheroids of large a/b (see Figs. 7 and 8 in Ref. 21), and it appears as an oscillation superimposed on the main oscillation in the extinction curves.

Figure 4 shows the cross sections for extinction, scattering, and absorption for absorbing prolate and oblate spheroids with $\tilde{m} = 1.33 + 0.05i$ and $a/b = 5$. The cross sections normalized by πr_V^2 are plotted against the equivalent size parameter $2\pi r_V/\lambda$. For large sizes ($2\pi r_V/\lambda \geq 5$), the scattering and extinction cross sections for both slender prolate spheroids and thin oblate spheroids are larger than are those of the volume equivalent spheres. On the other hand, the absorption cross sections of the spheroids and spheres are almost equal and independent of particle shapes in the size range shown in the figure. As pointed out by van de Hulst,[22] the absorption cross section is proportional to the volume of scatter for $4\pi n_i r/\lambda < 1$, where n_i is the imaginary part of the refractive index. Thus, the single scattering albedo of the randomly oriented spheroidal particles tends to be larger than that of the volume equivalent spheres.

Modifying the Mie theory in order to remove resonance effects due to surface waves, Chylek[27] proposed an empirical method to calculate the scattering properties of irregularly shaped, randomly oriented particles. The approximate method succeeded in reproducing the characteristic angular scattering pattern[18] measured for aerosol particles and has been applied to scattering from Martian dust.[28] However, a direct application of the method for absorbing particles brings a fictitious, abnormally large absorption even for very weakly absorbing particles,[29,30] because the modified Mie formalism is not energy-conservative.[31] In addition, this approximation cannot predict the phase shift of the efficiency curves for extinction and scattering.

Figure 5 shows the averaged asymmetry factor $\overline{\langle\cos\Theta\rangle}$ as a function of the size parameter $2\pi r_V/\lambda$ for the volume equivalent spheres for randomly oriented prolate and oblate spheroids with $\tilde{m} = 1.33$. Curves of $\overline{\langle\cos\Theta\rangle}$ vary following the oscillations in the curves of $\overline{C_{ext}}/\pi r_V^2$ in Fig. 2, but the amplitudes of the variations are much smaller, especially for spheroids with larger a/b than for those in the extinction curves. Except for the minimum

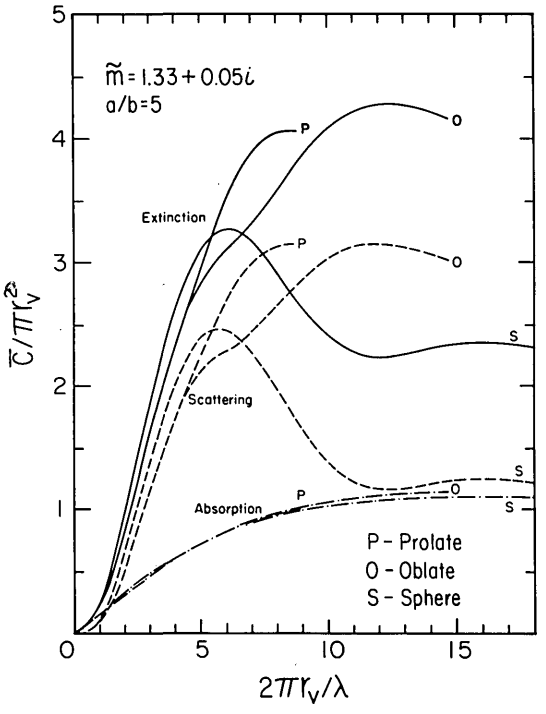

Fig. 4. Average cross sections for extinction, scattering, and absorption, normalized by the cross-sectional area πr_V^2 of the volume equivalent spheres as a function of the equivalent size parameter $2\pi r_V/\lambda$ for randomly oriented absorbing prolate and oblate spheroids with $\tilde{m} = 1.33 + 0.05i$ and $a/b = 5$. The cross sections for spheres, calculated with $r_{eq} = r_V$ and $v_{eff} = 0.01$ in the size distribution Eq. (28), are also shown.

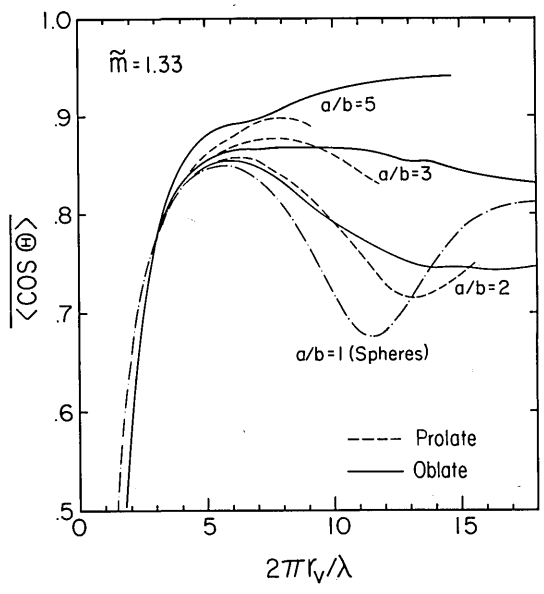

Fig. 5. Averaged asymmetry factor $\overline{\langle\cos\Theta\rangle}$, as a function of size parameter $2\pi r_V/\lambda$ for the volume equivalent spheres, for randomly oriented prolate and oblate spheroids with $\tilde{m} = 1.33$ and $a/b = 2$, 3, and 5. $\overline{\langle\cos\Theta\rangle}$ for spheres is also shown and calculated with $r_{eq} = r_V$ and $v_{eff} = 0.01$ in the size distribution Eq. (28).

regions of $\overline{\langle\cos\Theta\rangle}$ for spheroids of $a/b \lesssim 2$, $\overline{\langle\cos\Theta\rangle}$ of spheroidal particles is larger than it is for the equivalent spheres.

For a large particle, the asymmetry factor is primarily contributed by the scattering at small scattering angles,[32] and the forward scattering is composed primarily of three components: those due to diffraction, external (Fresnel) reflection, and transmission with two refractions. For randomly oriented nonspherical particles, the first component depends on the average projected area of the particles or equivalently on r_G.[5,22] The transmitted light may concentrate in the direction of smaller scattering angles for nonspherical particles than it does in the case of spherical particles.[5] In addition, for thin oblate spheroids, the forward scattering is still intensified by effects of grazing reflection. Actually, as will be seen later, the forward scattering of randomly oriented spheroids, except for thin oblate spheroids, is very close to that of the area equivalent spheres. On the other hand, for backscattering, the angular distribution of scattered intensity is rather flat, lacking a strong enhancement at backscattering, which is commonly observed in the scattering from spherical particles and negatively contributes to the asymmetry factor. As a result, the asymmetry factor of randomly oriented spheroidal particles tends to be larger than that of the equivalent spheres. Concerning this point, the result of Pollack and Cuzzi[19] by a semiempirical theory, disagrees with the present result. They obtained smaller values of $\overline{\langle\cos\Theta\rangle}$ even for flat platelike particles than those obtained for the volume equivalent spheres by choosing a parameter value of the forward scattering to backscattering ratio from measurements.[6,33] However, one should be careful in adopting experimental data, because the scattering measurements close to $\Theta = 0°$ and 180° are not available by using nephelometers.

B. Scattering Matrix Elements

Although it is difficult to deduce general characteristics of the scattering matrix for randomly oriented nonspherical particles from measurements[1–4,6,8,10] because of differences in models and experimental accuracy, some characteristic features can be deduced as follows: (a) the scattering matrix has the symmetrical form as in Eq. (13); (b) the phase function P_{11} has a rather flat angular distribution from side to backscattering; (c) $P_{22} < P_{11}$; (d) $P_{33} \neq P_{44}$; and (e) $P_{12} \lesssim 0$ for some sizes and angles for which $P_{12} > 0$ for equivalent spheres.

Present calculations for randomly oriented spheroidal particles with $\tilde{m} = 1.33$ and of the maximum dimension $\alpha = 15$ confirm all these characteristics. In Figs. 6–9 angular distributions of elements of the normalized scattering matrix are illustrated for prolate and oblate spheroids of $a/b = 5$ and 2, respectively. In each figure, (a) represents the normalized phase function P_{11}, (b) represents the degree of linear polarization $-P_{12}/P_{11}$ and P_{22}/P_{11}, (c) represents P_{43}/P_{11}, and (d) represents P_{33}/P_{11} and P_{44}/P_{11}. In the figures the scattering matrix elements of the area equivalent spheres are also shown by dotted lines. The figures are in increasing order of the size of the equivalent spheres.

1. P_{11}

Some characteristics of the normalized phase functions of randomly oriented spheroids are observed in the backscattering regions, that is, a rather flat angular distribution with a weak increase at the backscattering. Features such as the cloudbow and glory produced by scattering from large spheres are greatly reduced for spheroids of large a/b. It depends upon the shape parameter a/b whether randomly oriented spheroids will generate a more intense side scattering than will the equivalent spheres. The forward diffraction lobe of the equivalent spheres provides a fairly good approximation to that of the spheroids, except for the thin oblate spheroids of $a/b = 5$. The forward scattering from large, thin oblate spheroids is stronger, while the backscattering is very small: this scattering pattern yields a large asymmetry factor $\overline{\langle\cos\Theta\rangle}$ for thin oblate spheroids (Fig. 5).

2. $-P_{12}/P_{11}$

This element gives the degree of linear polarization $p = -P_{12}/P_{11}$ for single scattering of unpolarized incident light. The degree of polarization of randomly oriented spheroids with $a/b = 2$ is very close to that of the equivalent spheres for small scattering angles $\Theta \lesssim 70°$; however, with increasing scattering angles, it becomes positive at much smaller angles than it does in the case of spheres. This tendency is more dominant for spheroids with $a/b = 5$, for which p is positive over a wide range of scattering angles at which p for spheres is negative.

3. P_{22}/P_{11}

This element represents a ratio of the intensity component depolarized or cross polarized to the total scattered intensity. The depolarization ratio for total intensity is given here by

$$\Delta = (1 - P_{22}/P_{11}) = \frac{2Q_{12}}{\frac{1}{2}(Q_{11} + 2Q_{12} + Q_{22})}. \tag{29}$$

The depolarization ratio is a measure of nonsphericity because $P_{22} = P_{11}$ and $\Delta = 0$ for homogeneous spheres. For small angles $\Theta \lesssim 45°$, Δ is very small, especially for spheroids of $a/b = 2$. On the other hand, from side to backscattering, Δ is larger for spheroids of $a/b = 2$ than it is for $a/b = 5$, and the maximum depolarization appears at larger scattering angles for $a/b = 2$ than it does for $a/b = 5$. It is interesting that the maximum depolarization is largest for spheroids of $a/b \sim 2$ and that depolarization for spheroids of a/b smaller or larger than $a/b \sim 2$ decreases as $a/b \to 1$ or ∞. The linear polarization and depolarization will be further discussed later in relation to applications of scattering in the atmosphere.

4. P_{43}/P_{11}

For small scattering angles, the element for randomly oriented spheroids is close to that for the equivalent

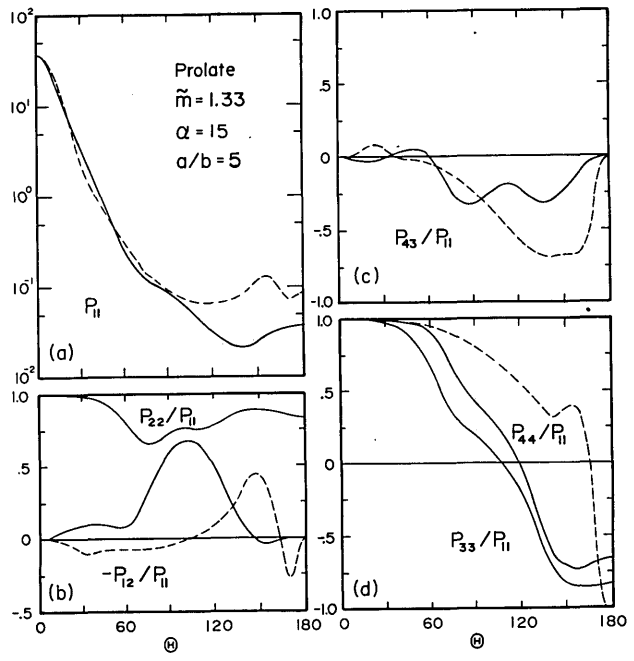

Fig. 6. Angular distribution of elements of the normalized scattering matrix for randomly oriented prolate spheroids with $\tilde{m} = 1.33$, $\alpha = 15$, and $a/b = 5$: (a) represents the normalized phase function P_{11}; (b) represents P_{22}/P_{11} and the degree of linear polarization $-P_{12}/P_{11}$; (c) represents P_{43}/P_{11}; and (d) represents P_{33}/P_{11} and P_{44}/P_{11}. The scattering matrix elements for the area equivalent spheres, shown by dotted lines, are calculated with $r_{eq} = r_G$ and $v_{eff} = 0.05$ in the size distribution Eq. (28).

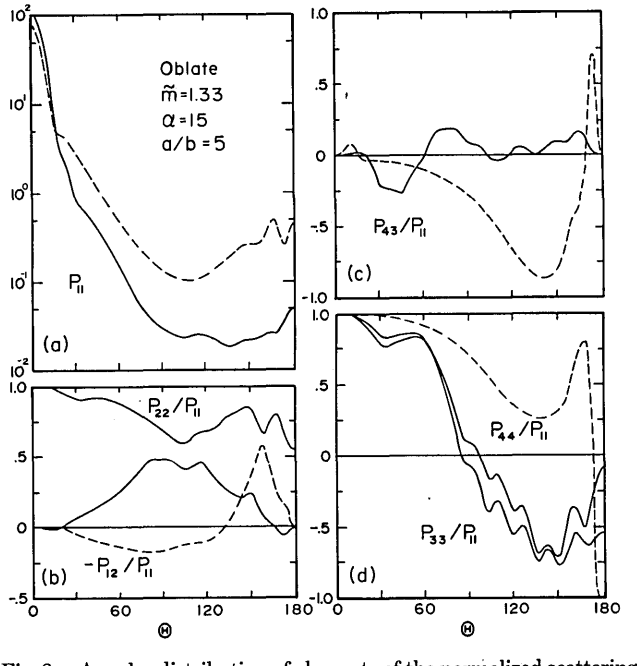

Fig. 8. Angular distribution of elements of the normalized scattering matrix for randomly oriented oblate spheroids with $\tilde{m} = 1.33$, $\alpha = 15$, and $a/b = 5$: (a) represents the normalized phase function P_{11}; (b) represents P_{22}/P_{11} and the degree of linear polarization $-P_{12}/P_{11}$; (c) represents P_{43}/P_{11}; and (d) represents P_{33}/P_{11} and P_{44}/P_{11}. The scattering matrix elements for the area equivalent spheres, shown by dotted lines, are calculated with $r_{eq} = r_G$ and $v_{eff} = 0.05$ in the size distribution Eq. (28).

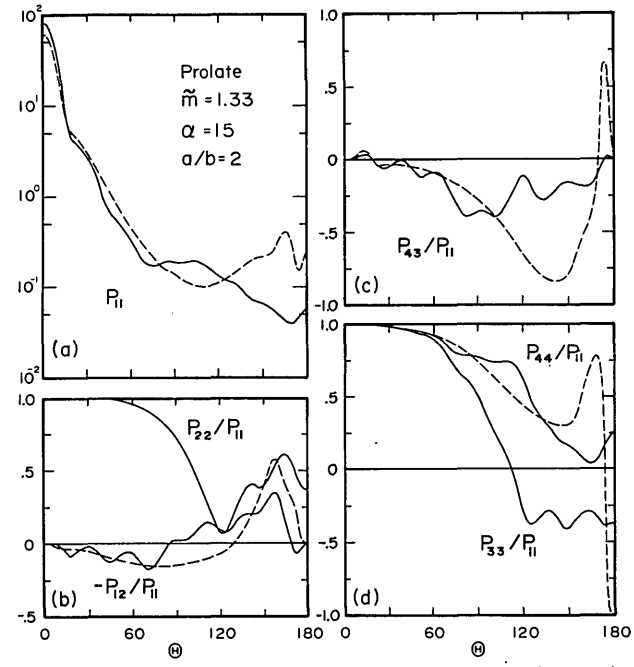

Fig. 7. Angular distribution of elements of the normalized scattering matrix for randomly oriented prolate spheroids with $\tilde{m} = 1.33$, $\alpha = 15$, and $a/b = 2$: (a) represents the normalized phase function P_{11}; (b) represents P_{22}/P_{11} and the degree of linear polarization $-P_{12}/P_{11}$; (c) represents P_{43}/P_{11}; and (d) represents P_{33}/P_{11} and P_{44}/P_{11}. The scattering matrix elements for the area equivalent spheres, shown by dotted lines, are calculated with $r_{eq} = r_G$ and $v_{eff} = 0.05$ in the size distribution Eq. (28).

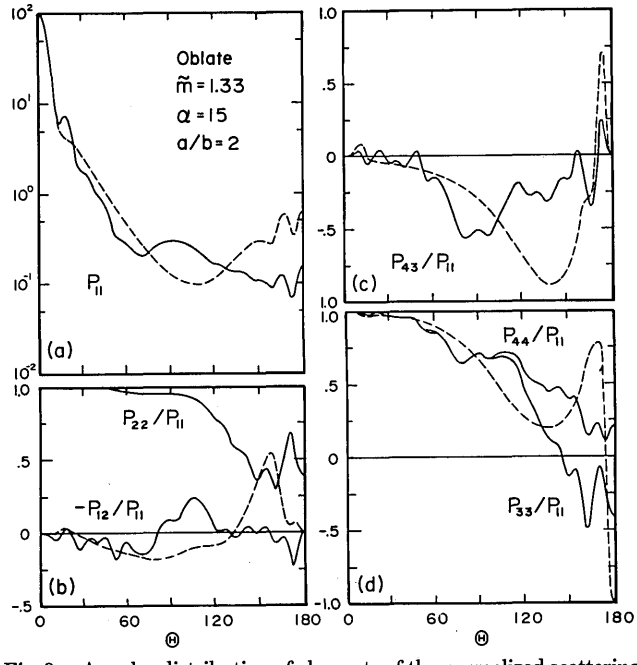

Fig. 9. Angular distribution of elements of the normalized scattering matrix for randomly oriented oblate spheroids with $\tilde{m} = 1.33$, $\alpha = 15$, and $a/b = 2$: (a) represents the normalized phase function P_{11}; (b) represents P_{22}/P_{11} and the degree of linear polarization $-P_{12}/P_{11}$; (c) represents P_{43}/P_{11}; and (d) represents P_{33}/P_{11} and P_{44}/P_{11}. The scattering matrix elements for the area equivalent spheres, shown by dotted lines, are calculated with $r_{eq} = r_G$ and $v_{eff} = 0.05$ in the size distribution Eq. (28).

spheres, and the good agreement extends to larger scattering angles than in the case of the degree of linear polarization, especially for spheroids of $a/b = 2$. This tendency of P_{43}/P_{11} has been noticed by Perry *et al.*[8] in the measurements for cubic particles of sodium chloride. For large scattering angles, however, P_{43}/P_{11} for spheroids, particularly for thin oblate spheroids of $a/b = 5$, is larger than it is for the equivalent spheres. The behavior of P_{43}/P_{11} for the thin oblate spheroid is in good agreement, except for small scattering angles, with the measurements of Holland and Gagne[6] for randomly oriented, flat platelike particles.

5. P_{33}/P_{11} and P_{44}/P_{11}

For randomly oriented spheroids, P_{44}/P_{11} is, in general, larger than P_{33}/P_{11}. The case of the thin oblate spheroids is an exception: crossing of curves of P_{33} and P_{44} is also seen in the results of Holland and Gagne.[6] We found that the difference between P_{44}/P_{11} and P_{33}/P_{11} changes with angle in a manner similar to P_{22}/P_{11} and that $\Delta \geq |P_{44} - P_{33}|/P_{11}$ with the equality valid at $\Theta = 0°$ and 180°. Perry *et al.*[8] noticed the inequality relationship $(P_{11} - P_{22}) > (P_{44} - P_{33}) > 0$ for NaCl particles. From the factor that $P_{33} = P_{44}$ for homogeneous isotropic spheres that yield no depolarization and from the structure of the transformation matrix Eq. (5), we can expect that $(P_{44} - P_{33})$ depends upon depolarizing components. At $\Theta = 0°$ and 180°, as predicted from the symmetry relations discussed by van de Hulst,[22] $P_{33} = \pm P_{22}$; from this combined with the equality mentioned above, we have $P_{44}/P_{11} = \pm(2P_{22}/P_{11} - 1)$, where the plus sign refers to $\Theta = 0°$, and the minus sign refers to $\Theta = 180°$.

In summary, the angular scattering behavior of randomly oriented spheroidal particles is much different from that of spheres at large scattering angles. It is interesting that, although prolate and oblate spheroids of the same a/b have similar scattering properties, prolate spheroids look more like spheres than do oblate spheroids.

IV. Applications and Discussions

A. Degree of Linear Polarization

Since the scattering properties, such as angular distribution of intensity, degree of polarization, and backscattering cross section, and depolarization have been widely measured and used to infer sizes and physical properties of scatterers in planetary atmospheres, and since these properties are quite different for nonspherical particles and spherical particles, we shall discuss in some detail these scattering properties in relation to scattering in the earth and planetary atmospheres.

Figure 10 shows the normalized phase function P_{11} and the degree of linear polarization p of thin oblate spheroids with $\tilde{m} = 1.33$ and $a/b = 5$ for three sizes: $\alpha = 5$, 10, and 20. Noticeable features are the strong forward scattering with weak backscattering and the positive polarization over a wide range of scattering angles. Slender prolate spheroids have similar features,

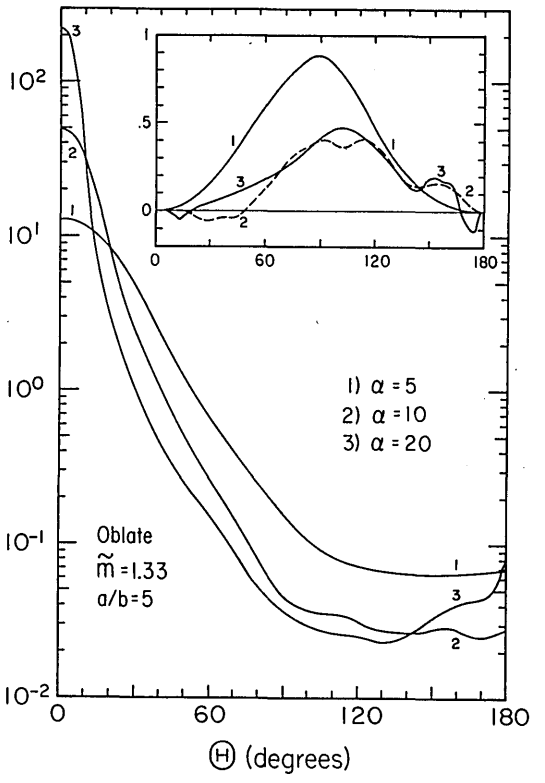

Fig. 10. Angular distribution of the normalized phase function P_{11} and the degree of linear polarization $-P_{12}/P_{11}$ (insert) for randomly oriented oblate spheroids with $\tilde{m} = 1.33$ and $a/b = 5$ for three sizes: $\alpha = 5$, 10, and 20.

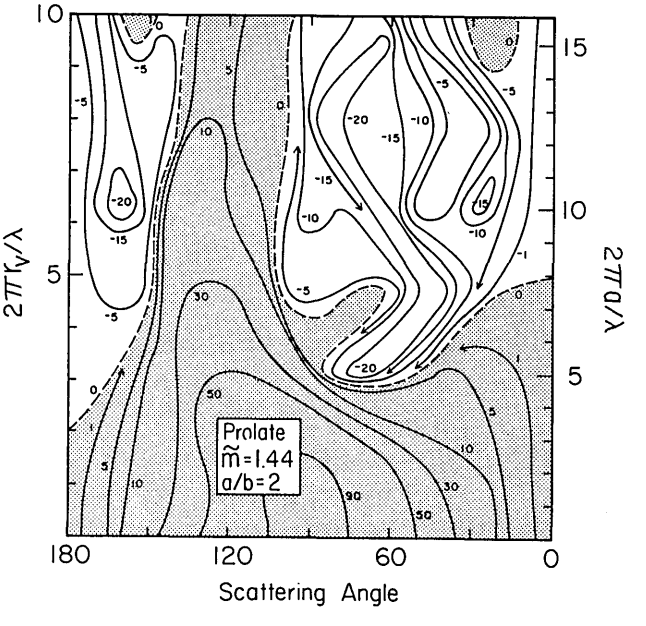

Fig. 11. Contour map of the percent of polarization, $-100\,P_{12}/P_{11}$, for single scattering of unpolarized incident light as functions of the scattering angle Θ and particle size for randomly oriented prolate spheroids with $\tilde{m} = 1.44$ and $a/b = 2$. Positive polarization regions are shaded.

as already shown in Fig. 6. Laboratory measurements by Huffman[9] and Dugin and Mirumyants[10] have shown positive polarization over $30° < \Theta < 150°$ for hexagonal columns and plates of ice crystals. The size of their particles are too large to be directly compared with our computed results in Fig. 10. A more suitable comparison is to compare the curves for $\alpha = 20$ in Fig. 10 with the measurements by Sassen and Liou[11] for small platelike crystals. They obtained positive polarization $0 < p < 0.3$ over $10° < \Theta < 170°$. The pattern of their normalized phase function agrees fairly well with the phase function of $\alpha = 20$ for $70° < \Theta < 170°$; however, for smaller angles of $10° < \Theta < 70°$, the slope of their phase function curve is flatter than is our slope. The disagreement is not surprising because their measurements are for polydisperse systems of ice crystals with different ratios of maximum-to-minimum dimensions (or a/b). Even though the shapes of the ice crystals are quite different from the shapes of the spheroids, it is interesting that thin oblate and slender prolate spheroids have scattering properties similar to those of ice crystals, except for features unique to hexagonal shapes such as the 22° halo.

Another example of the degree of linear polarization of nonspherical particles is illustrated in Fig. 11. In the figure, contours of the percent of linear polarization, $-100\,P_{12}/P_{11}$, are drawn for randomly oriented prolate spheroids with $\tilde{m} = 1.44$ and $a/b = 2$. The refractive index $\tilde{m} = 1.44$ is of a concentrated solution of sulfuric acid at $\lambda = 0.55\ \mu$m and was chosen to be compared with Fig. 3 in Ref. 34 or Fig. 17 in Ref. 24. The material is thought to be the composition of cloud particles in the high level clouds of Venus. By analyzing the linear polarization of sunlight reflected by Venus, Hansen and Hovenier[34] succeeded in determining the size distribution and refractive index of the cloud particles to within quite narrow limits. Their success is due to the cloud particles being nicely spherical. For spheres with $\tilde{m} = 1.44$, the linear polarization is negative at almost all scattering angles for sizes $4 < 2\pi r/\lambda < 10$.[24,34] For the prolate spheroids contrary to spheres, a wide bridge of positive polarization centered at $\Theta \sim 120°$ extends from the strong positive polarization region due to Rayleigh scattering by small particles. A similar positive polarization bridge was obtained for oblate spheroids with $\tilde{m} = 1.44$ and $a/b = 2$. The width of the bridge increases for spheroids of larger a/b (Fig. 10). From this theoretical study and the experimental results,[6–11] we conclude that nonspherical particles tend to have positive polarization at middle scattering angles.

From geometrical optics, the externally (Fresnel) reflected and internally reflected light contribute positively to the linear polarization; on the other hand, the transmitted light with two refractions has negative polarization.[22,24,35] Developing Hodkinson's[5] arguments on the difference between the scattering from an assembly of large, irregular particles and that from spheres in terms of geometrical optics, Coffeen[36] expected that the polarization of large, randomly oriented irregular particles may resemble that of spheres but with the negative polarization at small scattering angles compressed to only the smallest scattering angles, and with a general addition of positive polarization by internal reflections. His prediction is quite reasonable and agrees qualitatively with the present results, which suggest that twice-refracted light with negative polarization will concentrate at smaller scattering angles for spheroids of larger a/b. A rough ray tracing in the principal plane through the major and minor axes of spheroids seems to confirm this tendency. It suggests that the maximum deviation angle of the transmitted ray is smaller for thinner spheroids with larger a/b. In the limit of thin plane-parallel slabs, both the transmitted and internally twice-reflected light will appear in the direction of the incident light.

B. Backscattering and Depolarization

Figure 12 shows values of the normalized phase function for forward scattering ($\Theta = 0°$) and backscattering ($\Theta = 180°$) as a function of the particle size parameter α for prolate spheroids with $\tilde{m} = 1.33$ and $a/b = 2$. In the figures the backscattering depolarization component $\frac{1}{2}[P_{11}(180°) - P_{22}(180°)]$ is also plotted. Although the curve of the forward scattering $P_{11}(0°)$ is slightly shifted to larger sizes compared with the curve for the area equivalent spheres, the values are very close to each other. On the other hand, the backscattering $P_{11}(180°)$ of large spheroids is much smaller than that of the equivalent spheres. This low backscattering by

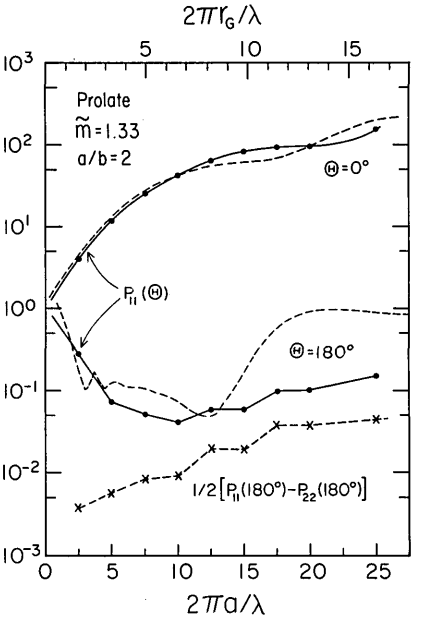

Fig. 12. Normalized phase functions at forward scattering, $P_{11}(0°)$, and backscattering, $P_{11}(180°)$, as a function of the size parameter $2/\pi a/\lambda$ for randomly oriented prolate spheroids with $\tilde{m} = 1.33$ and $a/b = 2$. The depolarization components at backscattering, $\frac{1}{2}[P_{11}(180°) - P_{22}(180°)]$, are also shown. $P_{11}(0°)$ and $P_{11}(180°)$ are compared with those for the area equivalent spheres; the latter are calculated with $r_{eq} = r_G$ and $v_{eff} = 0.01$ in the size distribution Eq. (28).

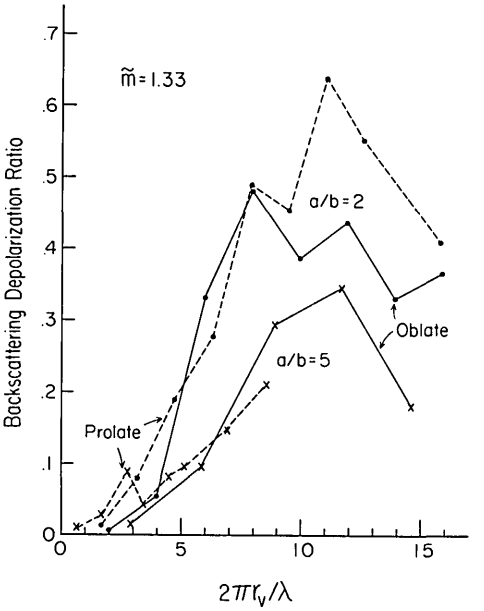

Fig. 13. Backscattering depolarization ratio, Eq. (30), as a function of size parameter $2\pi r_V/\lambda$ for the volume equivalent spheres for randomly oriented prolate and oblate spheroids with $\tilde{m} = 1.33$ and $a/b = 2$ and 5.

nonspherical particles will lead to underestimation of size and number density in an analysis using the Mie theory for the backscattering data measured by radar and lidar, if particles observed are in fact nonspherical.

The depolarized component increases with size in the size range shown in the figure. The ratio of the depolarized component to the polarized component at backscattering, i.e.,

$$\delta = [P_{11}(180°) - P_{22}(180°)]/[P_{11}(180°) + P_{22}(180°)], \quad (30)$$

is the backscattering depolarization ratio. At backscattering from randomly oriented spheroids, the depolarization ratio is independent of the polarization plane of the incident light, and δ has the same value as the linear depolarization ratios δ_H and δ_V, which will be discussed later. The backscattering depolarization ratio has been widely measured as a clear indication of nonsphericity of scatterers to investigate modification of aerosols with humidity,[37] to discriminate phases of hydrometers,[38–41] and to study microphysical properties[11,42–45] of cloud particles. In Fig. 13, the backscattering depolarization ratios δ are plotted for randomly oriented prolate and oblate spheroids with $\tilde{m} = 1.33$. As already mentioned, the backscattering depolarizations are larger for spheroids with $a/b = 2$ than they are for those with $a/b = 5$. For prolate and oblate spheroids of the same a/b, the values of δ are very similar. The present calculation of the backscattering depolarization ratio is limited to very small sizes compared with typical sizes of ice crystals; nevertheless, it is very interesting that our results for the dependence of the backscattering depolarization ratio on the shape factor a/b agree qualitatively with the measurements by Sassen of an increase of δ value for melting snowflakes[44] and for the dependence of δ distribution upon ice crystal habits;[45] he has obtained larger δ values for thicker ice crystals.

Measurements of the angular distribution of the depolarization ratios by laboratory experiments or bistatic remote sensing observations appear to have significant potential for inferring cloud composition.[11] We have discussed angular dependence of the depolarization components in Figs. 6–9, where P_{22}/P_{11} represents a portion of the cross-polarized components of the total scattered intensity. For practical use, however, a more convenient quantity is the linear depolarization ratio defined by the ratio of the cross-polarized component to the component that retains the same linear polarization as the incident light. The linear polarization ratios for incident light polarized parallel and perpendicular to the scattering plane are expressed by $\delta_H = Q_{12}/Q_{11}$ and $\delta_V = Q_{12}/Q_{22}$, respectively, in terms of the transformation matrix elements in Eq. (26). In Fig. 14, the linear depolarization ratios δ_H and δ_V are shown as a function of the scattering angle for randomly oriented oblate spheroids with the linear dimension $\alpha = 15$ and shape parameters $a/b = 2$ (left-hand side) and $a/b = 5$ (right-hand side). The figure clearly displays effects of particle shape on angular distributions of the linear depolarization and the degree of polarization. From the definition of the linear depolarization ratios, the degree of linear polarization is positive at scattering

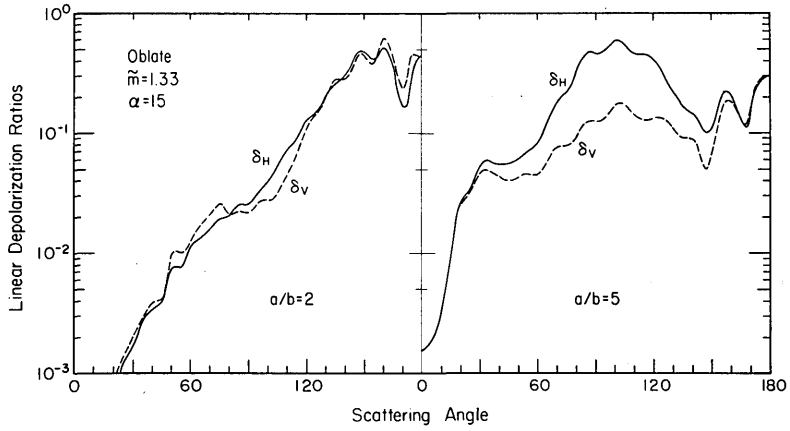

Fig. 14. Angular distribution of the linear depolarization ratios for randomly oriented oblate spheroids with the same size parameter, α = 15, but with different shape parameters, a/b = 2 (left-hand side) and a/b = 5 (right-hand side). The linear depolarization ratios, δ_H and δ_V, for the incidence of light polarized parallel and perpendicular to the scattering plane are shown by solid and dotted lines, respectively.

angles where $\delta_H > \delta_V$. Similar angular patterns of δ_H and δ_V have been obtained for randomly oriented prolate spheroids.

As regards the mechanism for backscattering depolarization from hexagonal ice crystals, Liou and Lahore[40] explained that the backscattering depolarization arises from a transformation of the vibration plane of the electric vector within the crystals through multiple internal reflections. They obtained a theoretical value of $\delta = 0.29$ for randomly oriented ice crystals. In laboratory and field experiments,[38,39,41,43–45] however, larger values of $\delta \geq 0.4$ have been frequently measured for the backscattering from randomly oriented ice crystals. Even homogeneous and isotropic nonspherical particles can produce large backscattering depolarization ratios, as shown in Fig. 13. Zerull,[33] attributed the origin of the cross polarization to total internal reflection. On total reflection, two linear polarization components, orthogonal to each other, undergo phase shifts of different amounts so that linearly polarized light will become elliptically polarized on total reflection.[46] For each component, the intensity of the totally reflected light is equal to the intensity of the incident light. However, no depolarized component appears only on total reflection, because the amplitude transformation matrix for total reflection has zero elements for the cross-polarization components in the form

$$\begin{bmatrix} \exp(i\varepsilon_{\parallel}) & 0 \\ 0 & \exp(i\varepsilon_{\perp}) \end{bmatrix},$$

where $\varepsilon_{\parallel}$ and $\varepsilon_{\perp}$ are the phase shifts for the polarization components parallel and perpendicular, respectively, to the plane of incidence.

Although the depolarization will be caused by different scattering mechanisms, the mechanisms should explain qualitatively and quantitatively the depolarization features observed in measurements[7,11,33,43–45] and computed in this study. A complete application of the ray tracing technique of geometrical optics to nonspherical particles, such as spheroids, would be very useful in understanding physical mechanisms involved in the scattering by nonspherical particles.

V. Concluding Remarks

A computational scheme has been developed to calculate the scattering properties of an ensemble of randomly oriented, identical spheroidal particles. The results obtained in this study will be applied not only to spheroidal particles but also to other nonspherical particles with smooth surfaces. These results explain measured characteristics of the scattering properties of randomly oriented nonspherical particles. One problem in our computation scheme is that it takes a long time to calculate the complete scattering matrix, e.g., about 3 h with an IBM 360/95 for oblate spheroids with $\tilde{m} = 1.33$, $a/b = 5$, and $\alpha = 15$ with the angular resolution $\Delta\Theta = \Delta\zeta = 2.5°$ and $\Delta\Phi = \Delta\chi = 5°$, which is one of the most difficult cases in the present calculation. However, the computer time could be shortened by further improvement of the computer program. The scattering and extinction cross sections and the asymmetry factor can be evaluated with much less computer time by our scheme.

The averaged extinction cross section, single scattering albedo, and asymmetry factor of randomly oriented spheroids tend to be larger than those of spheres of the same volume. This result is very important in evaluating radiative heat balance of the atmosphere and in estimating climatic effects of aerosols and ice clouds, because radiative transfer properties in the atmosphere are primarily described by those single scattering quantites.[47,48]

We found that spheroids tend to produce an angular distribution of scattered intensity with strong forward scattering and weak backscattering and with positive polarization at large scattering angles. Thus, in remote investigations of aerosols, use of the Mie theory for

scattering by spheres will yield erroneous results for the complex refractive index, with a large imaginary part or an underestimated real part, and for particle sizes with a distorted size distribution,[49] if nonspherical particles are in fact being measured.

The scattering properties of randomly oriented prolate and oblate spheroids of the same a/b are, in general, very similar. This implies that it will be difficult to discriminate between prolate and oblate shapes from a few sets of scattering data. However, a complete measurement of the scattering matrix will permit differentiation; see, for example, P_{43}, P_{33}, and P_{44} in Figs. 6–9.

The linear depolarization ratios increase with an increase of the scattering angle Θ and reach their maximum for $100° \lesssim \Theta \lesssim 160°$, as contributions of diffraction and external reflection decrease and those from internal reflections begin to dominate: the former two components do not involve any depolarization.[11] The maximum and backscattering depolarization ratios are largest for spheroids with $a/b \sim 2$, and they decrease as $a/b \to 1$ or ∞. For nonspherical particles with a refractive index close to 1 or with strong absorption, depolarization is very small,[16,33] because the contribution of multiple internal reflections to scattering by particles is very weak. A survey of angular patterns of the depolarization ratios and of the degree of polarization appear to be particularly promising for the inference of the shape parameter, like a/b for spheroids, of nonspherical particles.

We express our great appreciation to J. E. Hansen for useful discussions and his hospitality at the Institute for Space Studies. Without his generosity in providing computation time, it might have been impossible to finish this work. We also thank D. Coffeen, K. Kawabata, S. Limaye, and L. Travis for their useful comments and careful reading of our manuscript. During the course of this research, one of us (S.A.) held a NAS-NRC Postdoctoral Research Associateship and was on leave from the Geophysical Institute, Tohoku University, Japan.

References

1. B. S. Pritchard and W. G. Elliot, J. Opt. Soc. Am. **50,** 191 (1960).
2. G. I. Gorchakov and G. V. Rozenberg, Izv. Akad. Nauk SSSR Fiz. Atmos. Okeana **1,** 752 (1965).
3. V. A. Golovanev, G. I. Gorchakov, A. A. Yemilenko, and V. N. Sidorov, Izv. Akad. Nauk SSSR Fiz. Atmos. Okeana **7,** 857 (1971).
4. R. G. Quiney and A. I. Carswell, Appl. Opt. **11,** 1611 (1972).
5. J. R. Hodkinson, in *Electromagnetic Scattering ICES,* M. Kerker, Ed. (Macmillan, New York, 1963).
6. A. C. Holland and G. Gagne, Appl. Opt. **9,** 1113 (1970).
7. R. G. Pinnick, D. E. Carroll, and D. J. Hofmann, Appl. Opt. **15,** 384 (1976).
8. R. J. Perry, A. J. Hunt, and D. R. Huffman, Appl. Opt. **17,** 2700 (1978).
9. P. J. Huffman, J. Atmos. Sci. **27,** 1207 (1970).
10. V. P. Dugin and S. O. Mirumyants, Izv. Akad. Nauk SSSR Fiz. Atmos. Okeana **12,** 606 (1976).
11. K. Sassen and K.-N. Liou, J. Atmos. Sci. **36,** 838, 852 (1979).
12. Ye. A. Kadyshevich, Yu. S. Lyubovtseva, and I. N. Plakhina, Izv. Akad. Nauk SSSR Fiz. Atmos. Okeana **7,** 367 (1971).
13. Ye. A. Kadyshevich, Yu. S. Lyubovtseva, and G. V. Rozenberg, Izv. Akad. Nauk SSSR Fiz. Atmos. Okeana **12,** 106 (1976).
14. K.-N. Liou, J. Atmos. Sci. **29,** 524 (1972).
15. P. W. Barber and D.-S. Wang, Appl. Opt. **17,** 797 (1978).
16. M. Kotlarchyk, S.-H. Chen, and S. Asano, Appl. Opt. **18,** 2470 (1979).
17. K. G. Dedrick, A. R. Hessing, and G. J. Johnson, IEEE Trans. Antennas Propag. **AP-26,** 420 (1978).
18. P. Chylek, G. W. Grams, and R. G. Pinnick, Science **193,** 480 (1976).
19. J. B. Pollack and J. N. Cuzzi, in *Proceedings, Third Conference on Atmospheric Radiation, 28–30 June* (American Meteorological Society, New York, 1978).
20. S. Asano and G. Yamamoto, Appl. Opt. **14,** 29 (1975).
21. S. Asano, Appl. Opt. **18,** 712 (1979).
22. H. C. van de Hulst, *Light Scattering by Small Particles* (Wiley, New York, 1957), pp. 42–57, 110, 111, 172–183, and 200–233.
23. V. Vouk, Nature London **162,** 330 (1948).
24. J. E. Hansen and L. D. Travis, Space Sci. Rev. **16,** 527 (1974).
25. J. M. Greenberg and A. S. Meltzer, Astrophys. J. **132,** 667 (1960).
26. C. Rogers and P. G. Martin, Astrophys. J. **228,** 450 (1979).
27. P. Chýlek, J. Opt. Soc. Am. **66,** 285 (1976).
28. P. Chýlek and G. W. Grams, Icarus **36,** 198 (1978).
29. R. M. Welch and S. K. Cox, Appl. Opt. **17,** 3159 (1978).
30. C. Acquista, Appl. Opt. **17,** 3851 (1978).
31. P. Chýlek and R. G. Pinnick, Appl. Opt. **18,** 1123 (1979).
32. T. Nakajima and S. Asano, Sci. Rep. Tohoku Univ. Ser. 5: **24,** 89 (1977).
33. R. H. Zerull, Contrib. Atmos. Phys. **49,** 168 (1976).
34. J. E. Hansen and J. W. Hovenier, J. Atmos. Sci. **31,** 1137 (1974).
35. K.-N. Liou and J. E. Hansen, J. Atmos. Sci. **28,** 995 (1971).
36. D. L. Coffeen, Astron. J. **74,** 446 (1969).
37. D. W. Cooper, J. W. Davis, and R. L. Byers, J. Aerosol Sci. **5,** 117 (1974).
38. R. M. Schotland, K. Sassen, and R. Stone, J. Appl. Meteorol. **10,** 1011 (1971).
39. S. R. Pal and A. I. Carswell, Appl. Opt. **12,** 1530 (1973).
40. K.-N. Liou and H. Lahore, J. Appl. Meteorol. **13,** 257 (1974).
41. K. Sassen, J. Appl. Meteorol. **13,** 923 (1974).
42. C. M. R. Platt, J. Appl. Meteorol. **17,** 482 (1977).
43. K. Sassen, Appl. Opt. **16,** 1332 (1977).
44. K. Sassen, Nature London **255,** 316 (1975).
45. K. Sassen, J. Appl. Meteorol. **16,** 425 (1977).
46. M. Kerker, *The Scattering of Light* (Academic, New York, 1969), pp. 19 and 20.
47. S. Asano, M. Sato, and J. E. Hansen, NASA Conf. Publ. **2076,** 265 (1979).
48. W. M. Irvine, Icarus **25,** 175 (1975).
49. J. Heintzenberg, Contrib. Atmos. Phys. **51,** 91 (1978).